PAPER

Prospects of third-generation femtosecond laser technology in biological spectromicroscopy

IOP Publishing Journal of Optics
J. Opt. **20** (2018) 054005 (7pp) https://doi.org/10.1088/2040-8986/aab79a

Prospects of third-generation femtosecond laser technology in biological spectromicroscopy

Hanieh Fattahi[1,2,5], **Zohreh Fattahi**[3] **and Asghar Ghorbani**[4]

[1] Max-Planck Institut für Quantenoptik, Hans-Kopfermann-Str. 1, D-85748 Garching, Germany
[2] Physical and Theoretical Chemistry Laboratory, University of Oxford, South Parks Road, OX1 3QZ Oxford, United Kingdom
[3] Genetics Research Center, University of Social Welfare and Rehabilitation Sciences, Tehran, Iran
[4] Current address: Volkswagen Data:Lab, Ungererstr. 69, D-80805, München, Germany

E-mail: hanieh.fattahi@mpq.mpg.de

Received 3 October 2017, revised 18 February 2018
Accepted for publication 19 March 2018
Published 19 April 2018

Abstract

The next generation of biological imaging modalities will be a movement towards super-resolution, label-free approaches to realize subcellular images in a nonperturbative, non-invasive manner and towards new detection metrologies to reach a higher sensitivity and dynamic range. In this paper, we discuss how the third generation femtosecond laser technology in combination with the already existing concepts in time-resolved spectroscopy could fulfill the requirements of these exciting prospects. The expected enhanced specificity and sensitivity of the envisioned super-resolution microscope could lead us to a better understanding of the inter- and intra-cellular molecular transport and DNA-protein interaction.

Keywords: third-generation femtosecond laser technology, Yb:YAG oscillators, cognetive genomics, artificial intillegence, super-resolution microscopy, label-free microscopy, field-resolved metrology

(Some figures may appear in colour only in the online journal)

The beginning of modern natural sciences coincides with the invention of light microscopy [1]. In particular neuroscience has mainly been driven forward in the last 200 years by microscopic investigations [2] but still harbors the most complex secrets within the science of life.

Brain; the most complex organ in the human body is composed of 100 billion nerve cells acting in a complicated network of neuronal ensembles and is the basis for perception, emotion, memory, cognition, and intelligence. Human superiority over rest of the beings in Darwins evolution theory is due to the cognition and intelligence [3]. Intelligence as a complex polygenic trait is controlled by the mutual interaction of genes and environment [4, 5], where genes control the neuronal connectivity and networking by their differences at the genomic level and most importantly by their differential expression.

Among the approximate number of 25 000 known protein-coding genes in human, more than 70% are expressed in the brain controlling its development and functioning (see The Human Protein Atlas). It is shown that the genes distinguishing human from the other primates such as chimpanzee are highly expressed in the brain compared to the other tissues and organs. The involved genes in the development and functioning of the nervous system encode different types of proteins ranging from neurotransmitters, receptors, cytoskeleton and cell adhesion proteins to the ones involved in basic cellular mechanisms such as transcription factors [6]. Therefore, mapping the spatiotemporal action of genes in a living organism which contributes to normal functioning of the nervous system and especially the brain, is of great interest to understand the

[5] This article belongs to the special issue: Emerging Leaders, which features invited work from the best early-career researchers working within the scope of the *Journal of Optics*. Dr Hanieh Fattahi was selected by the Editorial Board of the *Journal of Optics* as an Emerging Leader.

molecular pathways and networks of genes and encoded proteins [7].

On the other hand, artificial intelligence (AI) in its early days has benefited extensively from neuroscience. A better understanding of the neural connections behind the learning process has a vital role in advancement of AI towards concepts like creativity, dreams, and, even consciousness [8] and can be used for validation of existing AI algorithms. What if the brain has anything similar to back-propagation [9]?

In recent years, the emergence of biologically inspired computing architectures, i.e. neuromorphic computing [10] has come to emulate brain-like ability to learn and adapt, in contrast to the canonical von Neumann computer architecture [11]. Some of the biggest challenges are a lack of knowledge in how exactly biological neural networks, memory, etc, work, and how neurons and glial cells store and process information. Also, understanding these processes could lead us towards merging AI with human intelligence via a brain–computer interface. This opportunity could in the short-term enable humans with neurodegenerative diseases, and in the long-term enhance human intelligence, memory and more direct interfacing with computing devices [12].

For decades, fluorescence microscopy has been a widespread tool to gain insights at the cellular level (cellular imaging) by detecting subcellular localization of proteins or their intracellular movements and distribution and also at the molecular level (molecular imaging) by observing single molecule dynamics and interactions in a living cell. Its specificity and sensitivity are afforded by large electronic transition dipole moments, and their background-free signal provides down to 200 nm spatial resolution. However, many of the proteins such as neurotransmitters or motor proteins are much smaller than the resolution of the microscope and intrinsically nonfluorescent and have to be labeled with fluorescent probes. The high weight molecular labels perturb the native function of the small molecules, and the observed functions do not necessarily reflect the behavior of the molecules at the sub-cellular level. Besides the applied biological bias due to the labeling, the number of labels that can be used simultaneously, is limited.

These limitations call for a novel label-free spectroscopy and imaging modality with an enhanced sensitivity to study the spatial distribution, concentration, and dynamics of small molecules and proteins at the subcellular level to enable mapping the entire neural circuits.

1. Label-free imaging modalities

For decades, vibrational microscopy has been a method of choice for label-free identification of different molecular compositions and structures. Vibrational microscopy based on infrared absorption or near-infrared (NIR) Raman scattering, offers intrinsic chemical selectivity due to the specific vibrational frequency of different molecules. Between the two, the NIR Raman microscopy has been more relevant for biological imaging, due to its higher spatial resolution and the negligible water absorption in visible and NIR spectral range [13].

In stimulated Raman scattering (SRS) the detected intensity loss/gain of the initial fields is proportional to the number of molecules and is not plagued by any non-resonant background emission, enabling the generation of a quantitative chemical map of the sample (figure 1(a)). However, the Raman effect is extremely weak with a typical photon conversion efficiencies lower than 1 in 10^8 photons, and the gain/loss appears on the initial spectrum of the interacting fields. Therefore, highly-sensitive detection schemes are required to resolve small changes in the signal. In 2008, Freudiger *et al* could successfully extract the SRS signal from the much larger background by modulating one of the narrowband excitation pulses using a lock-in amplifier [14, 15] leading to a successful label-free biological imaging [16, 17]. However, to measure the response of the entire molecular composition of a sample, the frequency of one of the excitation pulses has to be tuned, hence increasing the imaging acquisition time.

Alternatively, femtosecond broadband pulses have been used in place of the frequency scanned narrowband pulses to acquire the entire molecular fingerprint simultaneously (figure 1(b)). Successful implementation of broadband excitation pulses led to broadband CARS (M—or BCARS), where the anti-stokes signal is detected spectrally, or by measuring the molecular Raman free induction decay (RFID) temporally [18–20]. Nonetheless, broadband CARS (or CSRS) suffers from a low signal-to-noise ratio due to the presence of non-resonant background at these frequencies, which limits the detection sensitivity and distorting the Raman signal.

Inspired by impulsive stimulated Raman spectroscopy (ISRS) [21] and femtosecond stimulated Raman spectroscopy (FSRS) techniques in time-resolved spectroscopy [22], broadband excitation pulses have been used for SRS microscopy [23–25]. However, the spectral detection of the broadband gain/loss at megahertz (MHz) repetition rates which is required for video-rate imaging is challenging as multi-channel high-frequency detectors are not advanced yet. To overcome this issue and in a scheme proposed by Krausz *et al* [26], instead of spectral detection of the broadband gain/loss, the electric field of the RFID of the broadband excitation pulses can be temporally detected.

The detection of the electric field by means of electro-optic sampling or nonlinear photoconductive sampling has been a common method in terahertz spectroscopy. The metrology provides an unparalleled sensitivity and dynamic range which has been successful in detecting extremely faint signals such as vacuum fluctuation's field [27]. However, implementation of these techniques down to petahertz (PHz) frequencies has been limited due to the lack of a short probe pulse at PHz frequencies and MHz repetition rates.

In ISRS, the molecules are excited impulsively with a sudden, ultrashort pulse which is much briefer than the lifetime of molecular excitations. The excitation pulse is only present in a fraction of the vibrational oscillation period and delivers an impulsive force on molecules which initiates coherent vibrational motion in the ground electronic states, where the difference in energy is provided as vibrational

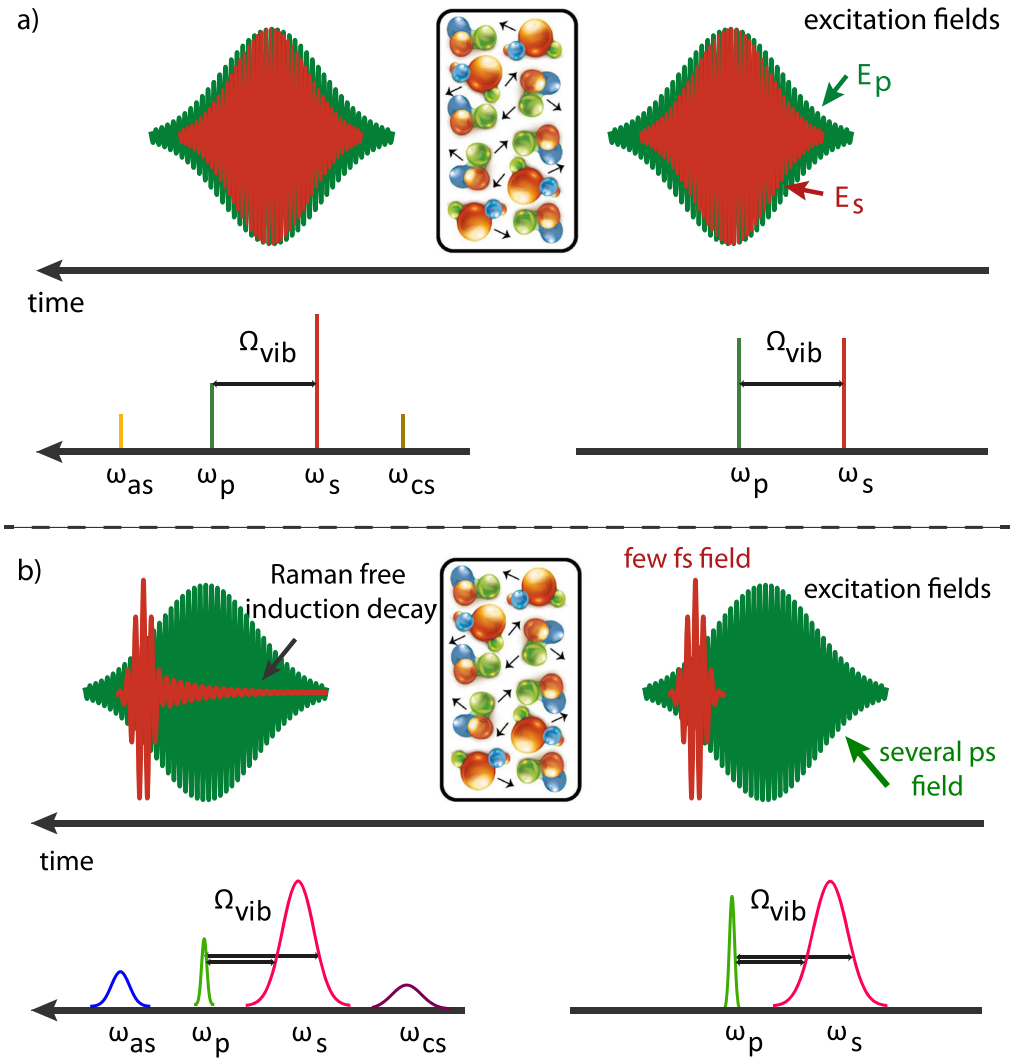

Figure 1. (a) Narrowband stimulated Raman scattering: two excitation fields with temporal duration of several ps initiate a Raman-active molecular vibrational coherence in a sample which decays with the vibrational dephasing time. Molecules are excited to a virtual energy state due to an oscillating polarization induced by an input field. This interaction leads to the absorption of energy (ω_p) by molecules and emission of a red-shifted scattered field/photons relative to the initial field (ω_s). Re-absorption of the initial field/photons at this stage can excite the molecule to a higher virtual energy level. This energy is released through the emission of a blue-shifted (ω_{as}) and red shifted (ω_{cs}) field/photons. The frequency of one of the excitation pulses is scanned to observe different vibrational modes of the sample. (b) Femtosecond stimulated Raman scattering: in this scheme, one of the narrowband excitation field is replaced with a broadband, femtosecond pulse and frequency tunning is not needed. The molecular fingerprint in both cases is retrieved from the spectral gain or loss of the excitation fields or the newly generated anti-Stokes and coherent Raman Stokes fields. Ω_{vib}: molecular vibrational frequency.

energy in the medium. As the excitation pulse is confined to several tens of femtosecond, the RFID is temporally separated and appears behind the ultrashort excitation pulses. Resolving the RFID, either by employing field-resolved techniques or by detecting the scattering of a third pulse interacting with the oscillating force in the medium [28], leads to a higher detection sensitivity and signal-to-noise ratio. This improvement is due to the confinement of the excitation pulse in a few femtosecond temporal window which allows for detection of RFID with a higher amplitude and therefore sensitivity as the molecular response decay exponentially (figure 1(b)).

In this case, stimulated scattering occurs through mixing among the continues distribution of Fourier components within the spectral bandwidth of the broadband pulse if the difference frequency of the frequency pairs in the ultrashort pulse matches the vibrational frequencies of the molecules in the sample. However, direct temporal detection of the RFID behind the excitation pulse and the corresponding retrieved Raman-shifts lacks molecular specificity, as here different intrapulse frequency-pair mixing, results in a similar Raman-shift (see figure 2(a)).

To break the degeneracy of the frequency mixing pathways of each molecular vibrational modes and to prevent the intrapulse SRS, the broadband excitation pulses should be temporally dispersed. The temporal pulse duration should be preferably equal or longer than the temporal period of the highest expected Raman-shift. The ultrashort pulses are then temporally overlapped with a narrowband excitation pulses in a scheme similar to FSRS. With this modification, the RFID is temporally separated from the broadband excitation pulse,

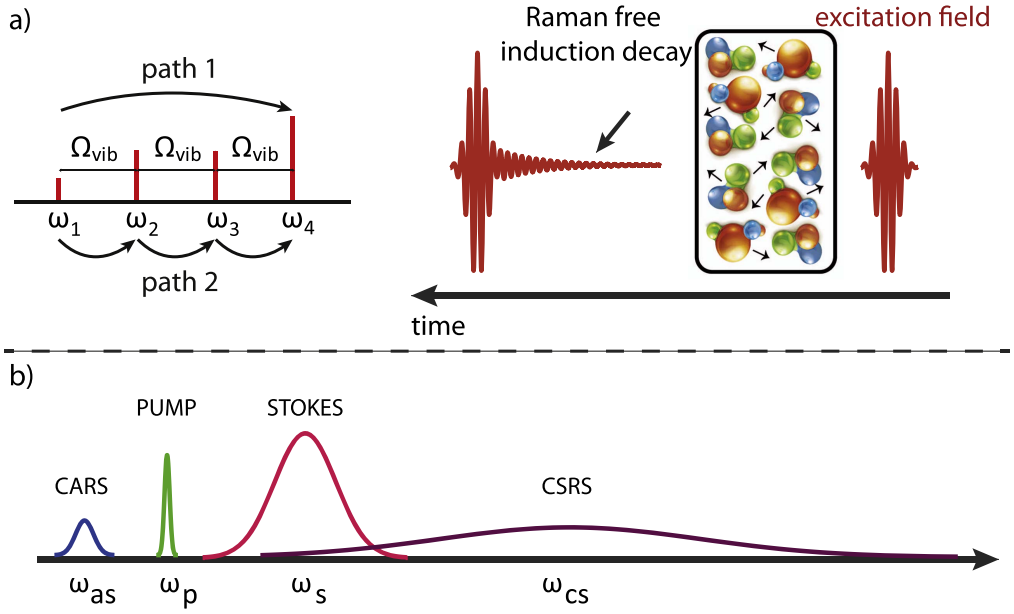

Figure 2. (a) Impulsive stimulated Raman scattering: a broadband excitation pulse is used for intrapulse stimulated Raman scattering. Temporal detection of RFID, in this case, suffers from a poor molecular specificity. For simplicity lets assume a broadband pulse consisting of four discrete frequencies (as shown in the left diagram). Two different paths, corresponding to two different vibrational frequencies, lead to absorption at ω_1 and emission at ω_4. In path 1, a molecular vibrational mode with the energy of $3\hbar\Omega_{vib}$ is stimulated, resulting in the absorption of one photon at ω_1 and emission at ω_4. In path 2, a vibrational mode of a molecule with the energy of $\hbar\omega$ is stimulated while a photon is absorbed at ω_1 and emitted at ω_2. Simultaneously, the second molecule with a similar vibrational mode, is absorbing a photon at ω_2 and emitting at ω_3, while for a third molecule the energy transfer happens between ω_3 and ω_4. The net energy transfer of this ensemble of molecules is absorption at ω_1 and emission at ω_4. Therefore, in paths 1 and 2, two different vibrational modes resulted in the same energy transfer, degrading the retrieved molecular specificity from the measured signal. (b) Spectral overlap of different scattering processes in broadband impulsive (intrapulse) stimulated Raman spectroscopy, results in degradation of the sensitivity and molecular specificity of the detected signal.

and the detected Raman-shifts correspond to specific molecular vibrations.

However, unlike the SRS with two narrowband excitation pulses, or an SRS scheme including a narrow-band and a heavily chirped broadband excitation pulses, the coherent oscillations continue even after the excitation pulses are gone. The RFID extends over 2–3 ps behind the excitation field corresponding to the dephasing time of the molecular vibrations in a condensed phase. The interaction between the coherent oscillation and the narrowband excitation pulse behind the broadband pulse, not only results in the SRS but also the generation of anti-Stokes or coherent-Stokes waves. As shown in figure 2(b), in broadband excitation the spectra of different scattering processes overlap, which degrades the vibrational specificity of the detected mode and makes the data analysis cumbersome. Moreover, the induced cross-phase modulation by the Kerr effect of the medium presents a background that is dependent on the optical alignment and collection efficiency of the broadband excitation pulses. By temporally offsetting the broadband excitation fields towards the trailing edge of the narrowband excitation pulse, the RFID can be isolated temporally. Moreover, the isolated RFID is not temporally overlapped with the narrowband excitation pulses which substantially suppress the generation of the anti-Stokes and coherent-Stokes fields in that temporal interval, resolving the issues raised by spectral overlap of different scattering processes (figure 3).

2. Current laser technology

To resolve the entire molecular vibrations of a biological sample, the difference frequency of the narrowband and broadband excitation pulses should cover four spectral regions: (i) fingerprint region, covering from ~500 to 1800 cm^{-1}, with approximately 90% of the biologically relevant vibrations active here, (ii) silent region, covering from ~1800 to 2700 cm^{-1}, attractive for evaluation of drug-cell interaction, its cellular uptake, and its release mechanism (iii) Bond region, covering from ~2700 to 3300 cm^{-1} and dominated by higher energy CH–/OH–stretch bond, and (iv) low frequency region [29].

Addressing all the Raman transitions requires broadband excitation pulses with ~3000 cm^{-1} spectral bandwidth. The spectral frequency of the narrowband pulse is chosen to fulfill the stimulated Raman condition: $\nu_{bb} - \nu_{nb} = \nu_{vib}$, where ν_{bb} is the frequency of the broadband pulse and ν_{nb} the frequency of the narrowband pulse. The Raman loss is observed for $\nu_{bb} > \nu_{nb}$ and the Raman gain for $\nu_{bb} < \nu_{nb}$.

In addition to the broad spectral coverage, the excitation pulses should be delivered at MHz repetition rates to allow for video-rate microscopy. In case of the field detection of RFID, the broadband excitation pulse and the probe pulse should be carrier-to-envelope phase (CEP) stable and cover the same spectral bandwidth.

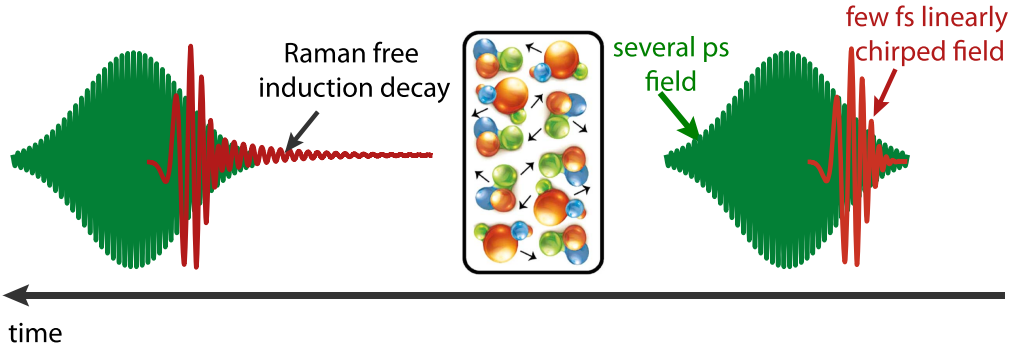

Figure 3. A broadband, few-cycle and a narrowband excitation fields initiate Raman-active molecular vibrational coherence in a sample. The broadband excitation pulse is slightly chirped to avoid intrapulse stimulated Raman scattering to assure the molecular specificity. The broadband and the narrowband excitation fields are temporally offset to eliminate the generation of anti-Stokes and coherent-Stokes fields behind the broadband excitation field, resolving the issues raised by spectral overlap of different scattering processes. The molecular fingerprint is retrieved from the detected Raman free induction decay.

Ti:Sa, Yb: and Er:fiber oscillators at MHz repetition rates have served as the frontend of many femtosecond stimulated Raman microscopes and multiplex SRS systems [30–32]. However, direct generation of broadband probe pulses with enough peak power for field-sampling from Ti:Sa lasers is impossible. Yb: and Er:fiber oscillators are delivering a higher peak power. They are compact and have a long-term stability, and their longer emission wavelength is compatible with biological applications. However, in comparison with solid-state sources, they have a higher noise-floor at above kilohertz frequencies.

Third generation femtosecond technology [33] based on Yb:YAG oscillators is now capable of delivering CEP-stable pulses with tens of microjoule energy at 1030 nm and MHz repetition rates. With a noise floor reaching below 10^{-8} at MHz frequencies [34], they are attractive sources for pushing biological imaging towards new frontiers such as field-resolved imaging if their spectrum can be extended to several octaves.

Supercontinuum generation (SC) in bulk is a suitable method for extending a narrowband spectrum over several octaves as it preserves the CEP stability. In SC generation based on Kerr nonlinearity, when the peak power of the laser exceeds the critical power of self-focusing, the initial spectrum is broadened dramatically [35]. At high average powers, which is the characteristic of Yb:YAG oscillators, tight focusing of the laser beam could lead to thermal damage of the nonlinear medium due to the high power density. Also, direct SC generation from Yb:YAG lasers is limited to the visible and NIR spectral range. SC generation at 1–2 μm is of biological interest as the probability of cellular photodamage decreases by increasing the excitation wavelength before the infrared absorption [36]. Covering this spectral range directly from Yb:YAG oscillators requires several nonlinear stages [37–39] and, consequently, requires higher input pulse energy, beyond the energy level delivered by the current MHz oscillators.

These limitations can be overcome by employing the quadratic, phase-mismatched cascaded nonlinearity of birefringent media [40] for SC generation. At a strong phase mismatch for second harmonic (SH) generation, a small fraction of the fundamental wave (FW) is converted to the SH waves in one coherence length and is converted back to the FW in the next coherence length. The phase shift between the back-converted and unconverted FWs induces a Kerr-like nonlinearity, which is controllable in both magnitude and sign through the phase mismatch value and can result in self-focusing or self-defocusing [41–43]. The enhanced effective nonlinearity offers the possibility to reduce the threshold peak intensity of SC generation to below the critical power [44].

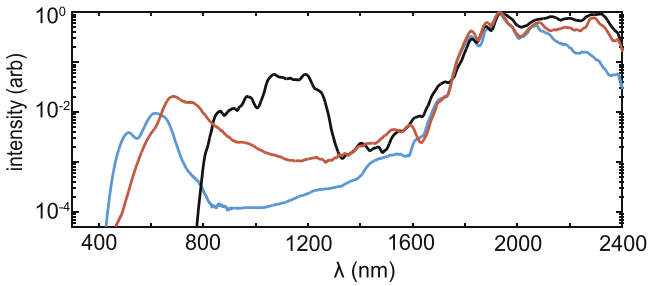

Figure 4. CEP-stable, Supercontinuum generation from 20 fs pulses centered at 2 μm. The red, black, and blue curves show the generated continuum in a 2 mm thick YAG, LNB, and the ordinary polarization of the BBO crystal. Each spectrum is normalized to one. The graph is taken from [47].

Figure 4 compares quadratic-cascaded SC generation in a $LiNbO_3$ (LNB) crystal and a beta barium borate (BBO) crystal [45, 46] to Kerr nonlinearity-driven SC in a YAG plate under similar initial conditions. The power spectral density of the newly generated frequencies in LNB is enhanced, and in comparison to BBO and YAG, the required critical power for SC generation in LNB in the self-focusing regime is lower by more than one order of magnitude. Pumping the nonlinear medium at its zero dispersion wavelength in LNB allows for a lower peak intensity threshold for SC generation and a higher power spectral density, rendering it as a suitable approach for SC generation from low peak power oscillators [47].

A frontend based on a CEP-stable, Yb-doped solid-state oscillator allows for generation of the narrowband and broadband excitation pulses, required for SRS, and the sampling few-cycle probe pulses required for EOS all from a

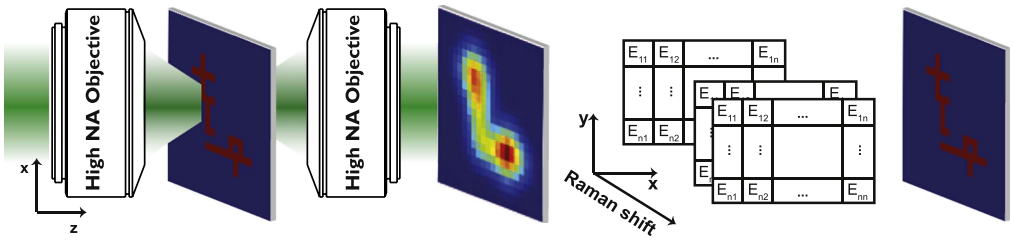

Figure 5. Simplified scheme of a field-resolved, label-free, super-resolution microscope. Raster-scanning of the excitation Raman pulses with a scanning step size smaller than the diameter of the focused beams provides super-resolution in the lateral dimension. The field-resolved detection increases the detection sensitivity and enables high resolution reconstruction of the center of mass of different molecules in the axial dimension.

single laser. Therefore, obviating the need for any additional temporal synchronization [48].

Field-detection of the broadband excitation pulses in SRS provides access to both the strength of the excited vibrations (amplitude) and the retardation with which they react to an external trigger (phase), paving the way for super-resolution, label-free imaging of biological samples.

3. Beyond the diffraction limit resolution

Most implementation of SRS microscopy attains resolution values at or above the diffraction limit. In diffraction-limited light microscopy, two objects with a separation much smaller than the illuminated area cannot be resolved and imaged accurately, and additional approaches must be utilized to achieve significantly improved resolution.

Based on a proposal by [49], depletion of the SRS signal, similar to stimulated emission depletion microscopy [50], provides a route towards super-resolution SRS imaging. In this approach, the sample is irradiated with a third toroidal-shaped beam, in addition to the two excitation beams. The third beam or the depletion beam turns off the SRS signal generation from the edges of the focal spot. The spatial resolution will scale with the probability of saturating the transition, therefore the power of the doughnut-shaped beam. However, the required high-intensity in this approach and other modalities based on depletion is not compatible with *in vivo* biological applications.

By increasing the detection sensitivity down to single molecule, the lateral spatial resolution can be increased by raster-scanning of the excitation Raman pulses with a scanning step sizes smaller than the diameter of the focused beams on the sample. In this approach, the measured stimulated Raman gain/loss of the two adjacent steps are subtracted, and the molecular information specific to the non-overlapping area is retrieved from the residual signal. The spatial resolution is proportional to the inverse of the scanning step size and is limited to the detection sensitivity (see figure 5).

Employing broadband excitation pulses decreases the scanning time for quantitative sub-cellular imaging of the entire molecular vibrational modes of the sample, substantially. In parallel, field-resolved detection of the signal keeps the promise for an enhanced detection-sensitivity. The recorded data form a three-dimensional matrix containing the lateral spatial information on x and y dimensions and the Raman active vibrational frequencies of the sample at the z-dimension. Therefore, the measured matrix has the unit of nm $\times$ nm $\times$ THz. The super-resolution quantitative image of the sample is then reconstructed by deconvolution of the complex-electric field at each element of the matrix.

Also, the measured complex-electric field of the signal contains molecular phase information or the retardation with which each molecular composition react to the external excitation. The phase information at each point of the matrix can, in principle, be used for enhancing the axial-spatial resolution. The measured relative phase of different Raman-shifts are related to the relative center-of-mass position of the associated molecular composition along the z-axis, providing additional information about the spatial distribution of different molecular compositions without the need for a raster scanning in the axial dimension.

4. Outlook

The next generation of laser-driven label-free biological microscopy requires a dramatic leap in sensitivity, dynamic range, and spatial resolution in a non-invasive manner. The third-generation femtosecond laser technology [33] combined with the three existing time-resolved spectro-microscopy methods: ISRS [21], FSRS [22] and field-resolved metrology [51] offers a new imaging modality.

The simultaneous label-free excitation of the entire molecular vibrational modes of the sample allows for a fast quantitative imaging. In parallel, the field detection of the temporally filtered RFID waves [26] keeps a promise for a higher detection sensitivity; a prerequisite for realizing the proposed label-free, super-resolution microscope in section 3. While Yb:YAG oscillators are an ideal frontend for such a microscope, the rapid development of solid-state oscillators towards operation at 2 μm and higher peak-powers [52] paves the way for even simpler imaging modalities with a lower cellular photodamage.

The described frontend in this paper offers a non-invasive, super-resolution imaging platform for *in vivo* investigation of inter- and intra-cellular molecular interaction in different biological systems, particularly, the neural system. The envisioned parameters in addition to the chemical selectivity of SRS, not only allows for a more accurate

mapping of protein and lipid densities [53] but also the DNA distribution based on O–P–O vibrations of the DNA backbone [54, 55].

In parallel, an accurate measurement of quantity and distribution of neurotransimitters [56] could lead to a better understanding of the function of biological networks and pathways involved in different neural system processes. The acquired knowledge does not only improve our understanding of the molecular basis of human cognition but also allows us to gain new insights into developing treatments by understanding the pathophysiology of many neurological and neurodegenerative diseases.

Acknowledgments

HF acknowledges support by the Minerva program of the Max Planck Society and thanks Ferenc Krausz for discussions regarding the field detection of molecular Raman free induction decay. HF and ZF would like to thank FM for years of support.

ORCID iDs

Hanieh Fattahi https://orcid.org/0000-0002-6485-529X

References

[1] Hell S W 2015 *Rev. Mod. Phys.* **87** 1169–81
[2] Wilt B A, Burns L D, Wei Ho E T, Ghosh K K, Mukamel E A and Schnitzer M J 2009 *Annu. Rev. Neurosci.* **32** 435–506
[3] Jacyna S 2009 *Brain* **132** 3481–7
[4] Franić S *et al* 2015 *Eur. J. Human Genet.* **23** 1378–83
[5] Tucker-Drob E M, Briley D A and Harden K P 2013 *Curr. Dir. Psychol. Sci.* **22** 349–55
[6] Androschuk A, Al-Jabri B and Bolduc F V 2015 *Frontiers Psychiatry* **6** 85
[7] Naumova O Y, Lee M, Rychkov S Y, Vlasova N V and Grigorenko E L 2013 *Child Dev.* **84** 76–88
[8] Hassabis D, Kumaran D, Summerfield C and Botvinick M 2017 *Neuron* **95** 245–58
[9] LeCun Y, Bengio Y and Hinton G 2015 *Nature* **521** 436–44
[10] Markram H 2006 *Nat. Rev. Neurosci.* **7** 153–60
[11] Schuman C D, Potok T E, Patton R M, Birdwell J D, Dean M E, Rose G S and Plank J S 2017 arXiv:1705.06963
[12] Harari Y N 2017 *Homo Deus: A History of Tomorrow* (London: Harvill Secker)
[13] Miller L, Smith G and Carr G 2003 *J. Biol. Phys.* **29** 219–30
[14] Owyoung A 1977 *Opt. Commun.* **22** 323–8
[15] Levine B, Shank C and Heritage J 1979 *IEEE J. Quantum Electron.* **15** 1418–32
[16] Freudiger C W, Min W, Saar B G, Lu S, Holtom G R, He C, Tsai J C, Kang J X and Xie X S 2008 *Science* **322** 1857–61
[17] Ozeki Y, Dake F, Kajiyama S, Fukui K and Itoh K 2009 *Opt. Express* **17** 3651–8
[18] Camp C H Jr and Cicerone M T 2015 *Nat. Photon.* **9** 295–305
[19] Volkmer A, Book L D and Xie X S 2002 *Appl. Phys. Lett.* **80** 1505–7
[20] Ideguchi T, Holzner S, Bernhardt B, Guelachvili G, Picqué N and Hänsch T W 2013 *Nature* **502** 355–8
[21] Dhar L, Rogers J A and Nelson K A 1994 *Chem. Rev.* **94** 157–93
[22] Frontiera R R and Mathies R A 2011 *Laser Photonics Rev.* **5** 102–13
[23] Ploetz E, Laimgruber S, Berner S, Zinth W and Gilch P 2007 *Appl. Phys.* B **87** 389–93
[24] Czerwinski L, Nixdorf J, Florio G D and Gilch P 2016 *Opt. Lett.* **41** 3021–4
[25] Fu D, Lu F K, Zhang X, Freudiger C, Pernik D R, Holtom G and Xie X S 2012 *J. Am. Chem. Soc.* **134** 3623–6
[26] Krausz F, Fattahi H, Huber M and Zigmann M 2017 Methods and devices for measuring changes in the polarization response of a sample by field-resolved vibrational spectroscopy *Patent*
[27] Riek C, Seletskiy D V, Moskalenko a S, Schmidt J F, Krauspe P, Eckart S, Eggert S, Burkard G and Leitenstorfer A 2015 *Science* **350** 420–3
[28] Ruhman S, aG J, Kohler B, Williams L and Nelson K 1987 *Rev. Phys. Appliquée* **22** 1717–34
[29] Raanan D, Ren L, Oron D and Silberberg Y 2018 *Opt. Lett.* **43** 470–3
[30] Beier H T, Noojin G D and Rockwell B A 2011 *Opt. Express* **19** 18885–92
[31] Dobner S, Cleff C, Fallnich C and Groß P 2012 *J. Chem. Phys.* **137** 174201–5
[32] Selm R, Winterhalder M, Zumbusch A, Krauss G, Hanke T, Sell A and Leitenstorfer A 2010 *Opt. Lett.* **35** 3282–4
[33] Fattahi H *et al* 2014 *Optica* **1** 45–63
[34] Huber M, Schweinberger W, Stutzki F, Limpert J, Pupeza I and Pronin O 2017 *Opt. Express* **25** 22499–509
[35] Silva F, Bates P K, Esteban-Martin A, Ebrahim-Zadeh M and Biegert J 2012 *Opt. Lett.* **37** 933–5
[36] Squirrell J M, Wokosin D L, White J G and Bavister B D 1999 *Nat. Biotechnol.* **17** 763–7
[37] Fattahi H, Wang H, Alismail A, Arisholm G, Pervak V, Azzeer A M and Krausz F 2016 *Opt. Express* **24** 24337–46
[38] Fattahi H, Schwarz A, Keiber S and Karpowicz N 2013 *Opt. Lett.* **38** 4216–9
[39] Alismail A, Wang H, Altwaijry N and Fattahi H 2017 *Appl. Opt.* **56** 4990–4
[40] Zhou B B, Chong A, Wise F W and Bache M 2012 *Phys. Rev. Lett.* **109** 4499–503
[41] Krupa K, Labruyère A, Tonello A, Shalaby B M, Couderc V, Baronio F and Aceves A B 2015 *Optica* **2** 1058–64
[42] Šuminas R, Tamošauskas G, Jukna V, Couairon A and Dubietis A 2017 *Opt. Express* **25** 6746–56
[43] Beckwitt K, Wise F W, Qian L, Walker L A and Canto-Said E 2001 *Opt. Lett.* **26** 1696–8
[44] Šuminas R, Tamošauskas G, Valiulis G and Dubietis A 2016 *Opt. Lett.* **41** 2097–100
[45] Zhou B, Guo H and Bache M 2015 *Opt. Express* **23** 6924– 6936
[46] Zhou B and Bache M 2015 *Opt. Lett.* **40** 4257–60
[47] Wang H, Alismail A, Barbiero G, Wendl M and Fattahi H 2017 *Opt. Lett.* **42** 2595–8
[48] Fattahi H *et al* 2012 *Opt. Express* **20** 9833–40
[49] Silva W R, Graefe C T and Frontiera R R 2016 *ACS Photonics* **3** 79–86
[50] Hell S W and Wichmann J 1994 *Opt. Lett.* **19** 780–2
[51] Kübler C, Huber R and Leitenstorfer A 2005 *Semicond. Sci. Technol.* **20** S128–33
[52] Zhang C *et al* 2017 *Optica* **4** 103–9
[53] Freudiger C W, Min W, Holtom G R, Xu B, Dantus M and Sunney Xie X 2011 *Nat. Photon.* **5** 103–9
[54] Lu F K *et al* 2015 *Proc. Natl. Acad. Sci.* **112** 11624–9
[55] Zhang X, Roeffaers M B J, Basu S, Daniele J R, Fu D, Freudiger C W, Holtom G R and Xie X S 2012 *ChemPhysChem* **13** 1054–9
[56] Fu D, Yang W and Xie X S 2017 *J. Am. Chem. Soc.* **139** 583–6